Pergamon

Acta mater. 48 (2000) 4281–4291

Acta MATERIALIA

www.elsevier.com/locate/actamat

MICROSTRUCTURE AND PERFORMANCE OF A CERMET MATERIAL HEAT-TREATED IN NITROGEN

J. ZACKRISSON[1]*, U. ROLANDER[2], B. JANSSON[2] and H. -O. ANDRÉN[1]

[1]Department of Experimental Physics, Chalmers University of Technology and Göteborg University, SE-412 96 Göteborg, Sweden and [2]AB Sandvik Coromant, SE-126 80 Stockholm, Sweden

(Received 1 July 1999; received in revised form 13 July 2000; accepted 13 July 2000)

Abstract—A Ti(C,N)–TiN–WC–Co cermet material was subjected to a heat-treatment in nitrogen which substantially improved the plastic deformation resistance during cutting. The microstructure was characterised using analytical electron microscopy. It was found that a surface zone rich in titanium and nitrogen was induced by the heat-treatment. The high nitrogen activity in the surface region was the driving force for outward transport of titanium and inward transport of tungsten in the cobalt binder. An irregularly shaped nitrogen-rich titanium carbonitride reprecipitated from the binder phase during the heat-treatment, often as surrounding layers on already existing carbonitride grains. The morphological change of the hard phase might explain the dramatically improved plastic deformation resistance by obstructing grain boundary sliding. The experimental findings were in accordance with thermodynamic calculations performed using the Thermo-Calc software.

Keywords: Analytical electron microscopy; Energy-filtered transmission electron microscopy (EFTEM); Microstructure; Thermodynamics; Mechanical properties

1. INTRODUCTION

Gradient structured cemented carbides have been the subject of research in the hardmetal industry for quite some time. Often, the purpose is to produce a coated cutting tool where the tungsten carbide based substrate material has a binder phase enrichment towards the surface. The idea is that the tough surface layer shall prevent cracks in the brittle coating from propagating into the substrate. Thereby, tool life would be prolonged. Several papers concerned with the formation of such cubic carbide-free surface regions have been published [1–4].

Lately, attention has been paid to titanium carbonitride based cermets with a gradient structure of a reverse nature, i.e. with a surface zone enriched in hard titanium carbonitride based phases and a lower volume fraction of tough binder phase [5, 6]. In this way, it is possible to achieve cutting properties similar to those of coated tool materials without having to coat the substrate.

The microstructure of a cermet material consists of hard carbonitride grains in a tough metallic binder phase. The carbonitride grains often have a core–rim structure [7, 8] with the composition depending on the starting powder mixture and the sintering process. Sometimes the rim is divided into an inner rim and an outer rim, where the former is enriched in heavier elements and lies between the core and the outer rim. Cermet microstructures are complex with relatively small grains ($\approx$0.5–1 μm) and a varying composition including carbon and nitrogen. These factors put requirements on the microanalytical techniques to be used. Accurate quantitative microanalysis of both light and heavy elements and a high spatial resolution have to be fulfilled at the same time. It should be noted that this cannot be achieved with electron microprobe analysis (EMPA) or energy dispersive X-ray analysis (EDX) in combination with scanning electron microscopy (SEM).

This paper is concerned with the detailed microstructure, thermodynamical calculations and performance data of a Ti(C,N)–TiN–WC–Co cermet material heat-treated in nitrogen. The heat-treatment introduced a compositional gradient towards the surface and the investigation has therefore mainly been concentrated on the surface zone. The methods used for the microstructural characterisation were scanning electron microscopy, electron microprobe analysis, transmission electron microscopy (TEM) and energy-filtered transmission electron microscopy (EFTEM). Quantitative high-resolution microanalysis was performed using electron energy-loss spectroscopy

* To whom all correspondence should be addressed.
E-mail address: jenni@fy.chalmers.se (J. Zackrisson)

PII: S1359-6454(00)00212-3

(EELS) and energy dispersive X-ray analysis in combination with TEM. The thermodynamics of this system were calculated utilising the Thermo-Calc software [9].

2. EXPERIMENTAL DETAILS

2.1. Materials

The material studied in this work was sintered at 1430°C for 90 min from a powder mixture of Ti(C,N), TiN, WC, cobalt and carbon black. The composition after sintering is given in Table 1. The post-sintering heat-treatment was performed in a nitrogen atmosphere at 1200°C for 20 h, and introduced a surface zone that from optical microscopy appeared to be approximately 20 μm thick.

2.2. Specimen preparation

Polished surfaces for the SEM and EMPA investigations were produced using standard specimen preparation techniques. Cross-section TEM specimens were fabricated by glueing the interesting surfaces together and cutting Ø3 mm disks with an ultrasonic cutter. A fine steel net with 15 μm diamond spray was used to polish the disks down to 100 μm thickness. The disks were then dimple ground using Gatan equipment and thinned to electron transparency by ion-milling in a Gatan DuoMill 600.

2.3. Electron microprobe analysis

Compositional depth profiles of the heat-treated and the as-sintered materials were acquired using a Jeol JXA8900R combined WD/ED microanalyser operated at 15 kV. The line scans were 100 μm wide, and considering the carbonitride grain size as being about 1 μm, this means that the composition given by the depth profiles is an average over many grains and thus a function of both composition and volume fraction of the different phases.

2.4. Scanning electron microscopy

Scanning electron microscopy was performed to obtain a general overview of the microstructure of the surface zone and the bulk of the heat-treated as well as of the as-sintered material. The instrument used was a CamScan S4-80DV operated at 12 kV and at a working distance of 10 mm for optimum resolution and signal-to-noise ratio of the backscattered electron signal.

Table 1. Composition of the investigated material after sintering (at%)

Co	C	N	O	Ti	W
11.20	29.48	14.39	0.33	39.90	4.71

2.5. Transmission electron microscopy

Transmission electron microscopy was used to study the microstructure in more detail and especially for microanalytical reasons. A Philips CM200 FEG-TEM equipped with a Gatan imaging filter (GIF) and a Link ISIS EDX system was used for the TEM work. Energy-filtered transmission electron microscopy provided the elemental distribution in the form of elemental maps or jump ratio images [10]. This gave an indication of the phase distribution at different depths from the surface. The phase compositions were analysed using energy dispersive X-ray analysis (metal content) and energy-loss spectroscopy (light element content) in the TEM. EELS spectra were acquired in TEM image mode to minimise the effect of carbon contamination and evaluated according to the procedure optimised for titanium based carbonitrides [11].

2.6. Thermodynamic calculations

The thermodynamic calculations have been carried out using version M of the Thermo-Calc software [9]. A first provisional version of a database for cemented carbides compiled by Dumitrescu [12] has been used for the thermodynamic description of the C–Co–N–Ti–W system. The so-called Calphad method is utilised for the thermodynamic calculations. The integral Gibbs energy is modelled for each phase separately. The equilibrium state is calculated numerically by minimising the appropriate free energy for the prescribed equlibrium conditions. In general, no closed mathematical expression for the activity of a component in a multi-phase system can be derived. The Calphad method is described in Refs [9, 12].

2.7. Performance testing

In order to evaluate how the surface gradients affect fundamental cutting tool properties turning tests were performed using TNMG160408-PF inserts with 30 μm edge radius. The heat-treatment dramatically improved the cutting performance. Consequently, it was not possible to use the same cutting conditions for the as-sintered as for the heat-treated cermet while maintaining reasonable tool-life values. Instead, a well-established PVD-coated grade within the P15 range for turning was chosen as the reference, rather than the investigated material in the as-sintered condition. The reference is characterised by good toughness and reasonable plastic deformation resistance.

Plastic deformation resistance was tested in longitudinal turning of steel (SS2541) without coolant. The cutting conditions were 275 m/min cutting speed, 0.2 mm/r feed, and 2 mm depth of cut. Under these conditions relatively soft cermets will deform by edge impression, leading to rapid flank wear (*VB*). The test was monitored by measuring the flank wear every 2.5 min and flank wear exceeding 0.3 mm or 15 min total cutting time were chosen as tool life criteria.

Toughness was tested in a facing operation with coolant. The work piece was a thick-walled cylindrical steel tube (SS2234) with 93 mm outer diameter and 57 mm inner diameter. Two flat surfaces, 38 mm in width, were produced on opposite sides of the periphery. In this way a gentle interrupted cut is obtained which stresses the thermal more than the mechanical properties of the cutting tool. The cutting conditions were 250 m/min cutting speed, 0.3 mm/r feed, and 0.5 mm depth of cut. The typical wear pattern under these conditions is formation and growth of thermal cracks on the rake face leading to fracture. The test was monitored by counting the number of passes needed to obtain fracture.

3. RESULTS

3.1. Microstructure

SEM micrographs of the surface zone of the heat-treated and as-sintered materials are shown in Fig. 1. The microstructure of the as-sintered material shows all features of a typical cermet microstructure. Hard carbonitride grains, often with a core–rim structure, are embedded in a tough metallic binder phase. The grain size of the binder ($\approx 10^3$ μm) is substantially larger than the carbonitride grain size (≈ 1 μm), and consequently one binder phase grain surrounds a large number of hard phase grains. The cores are Ti(C,N) that remain undissolved from the raw material powder [13]. During sintering, two mixed carbonitride phases (Ti,W)(C,N) with different tungsten contents have reprecipitated as a rim onto the Ti(C,N) cores. The inner rim, enriched in tungsten, is formed at a low nitrogen activity due to the open porosity during solid state sintering, and the outer rim is formed at a higher nitrogen activity during liquid phase sintering [14–17]. Close to the surface of the as-sintered material the microstructure is identical to that of the bulk, whereas the appearance of the surface zone (about 20 μm) of the heat-treated material is quite different. There seems to be a higher volume fraction of phases with low atomic weight close to the surface, but also small grains of a phase heavier than all the others present. None of these features is present in the as-sintered material.

The EMPA depth profiles (see Fig. 2) reveal that close to the surface the heat-treated material is enriched in titanium and nitrogen and depleted in tungsten and carbon. The titanium, tungsten, nitrogen and carbon contents are constant all through the as-sintered material. Further below the surface, the tungsten content of the heat-treated material is higher than in the as-sintered material. The cobalt content increases towards the surface but cannot be con-

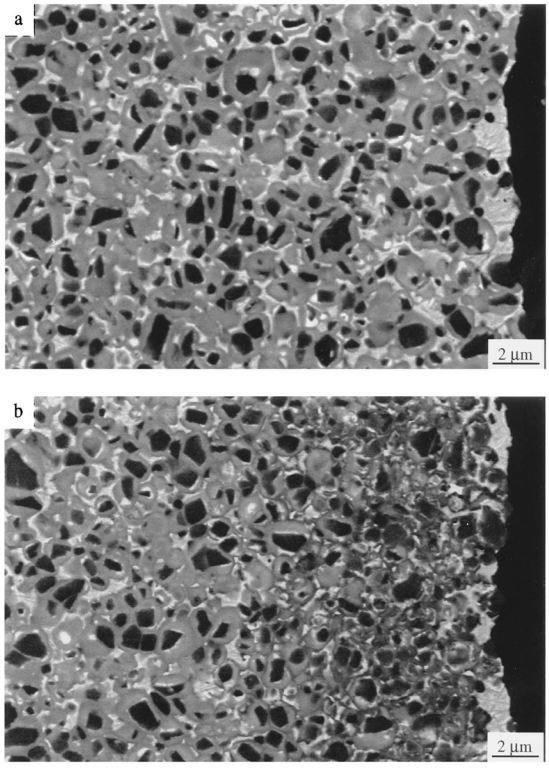

Fig. 1. SEM micrographs of the surface zones in (a) the as-sintered and (b) the heat-treated materials.

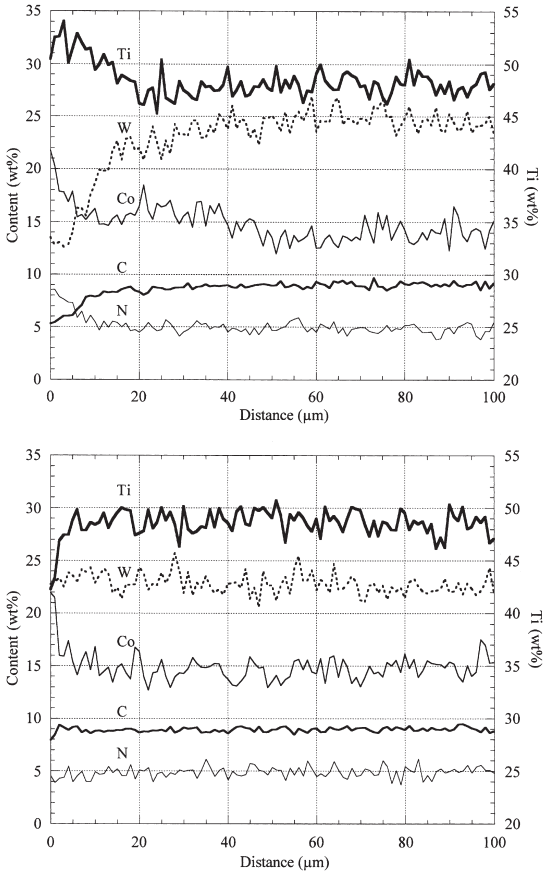

Fig. 2. Electron microprobe depth profiles from (a) the heat-treated and (b) the as-sintered materials. The titanium content is given on the right scale.

sidered to be a consequence of the heat-treatment alone since the as-sintered material shows a similar cobalt profile. However, in the heat-treated material there is also an increase in cobalt content between 15 and 40 μm below the surface, which is not seen in the as-sintered material.

EFTEM provides elemental distributions and was used to determine the presence and distribution of phases at different depths of the heat-treated and as-sintered materials. Figure 3 shows the distribution of cobalt, titanium, carbon, nitrogen and tungsten in the near-surface region of the heat-treated material. Figure 3a is an RGB image constructed from the titanium, nitrogen and tungsten jump ratio images. The advantage of RGB images is that the elemental distribution of more than one element can be displayed in one single image. By making an appropriate choice of elemental maps as the basis for the RGB image it is possible to extract the phase distribution from one image instead of trying to correlate five different elemental maps. RGB images for regions at different depths of the heat-treated material are shown

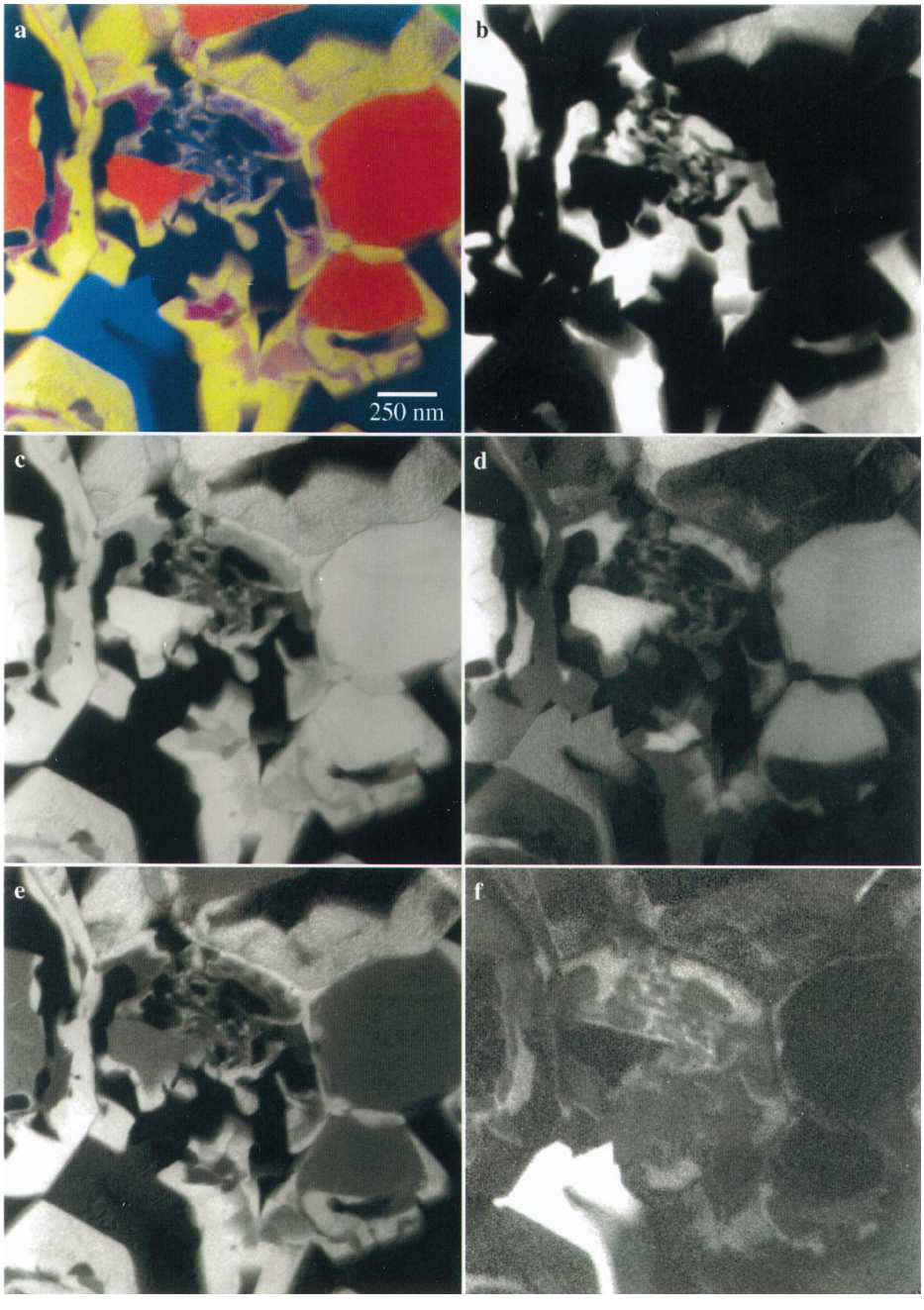

Fig. 3. (a) RGB image constructed from the titanium (red), nitrogen (green) and tungsten (blue) jump ratio images of a region in the surface zone of the heat-treated material. (b) Cobalt, (c) titanium, (d) carbon, (e) nitrogen, and (f) tungsten jump ratio images of the same region.

in Fig. 4. Apart from the phases usually present in cermet materials, the surface zone of the heat-treated material contained a nitrogen-rich phase and small tungsten carbide grains. The nitrogen-rich phase occurs frequently and surrounds the carbonitride grains in thin layers. At 100 and 150 μm below the surface of the heat-treated material, a tungsten-rich carbonitride phase was found to surround the carbonitride grains, see Fig. 5. None of these microstructural features were found in the as-sintered material, neither in the bulk nor in the surface zone. This figure also reveals that there is an enrichment of nitrogen in the core close to the core–rim boundary. This is not an effect of the heat-treatment since this nitrogen enrichment has been observed both in the as-sintered material and in other cermet materials [18, 19]. For comparison, Fig. 6 shows RGB images of the surface region and of the bulk of the as-sintered cermet material.

The phase compositions at different depths were determined by EDX and EELS in the TEM, see Tables 2–7. The binder contains mainly cobalt but also tungsten and titanium. The amount of tungsten and titanium dissolved in the binder phase decreases with increasing depth, from 8–9 at% in the near-surface region to 5 at% in the bulk. The core is a titanium carbonitride with the C+N content slightly decreasing with increasing depth. No major differences are found in the C/(C+N) ratio of cores at different depths. The outer rim is a (Ti,W)(C,N) phase for which the nitrogen content decreases with increasing depth. The tungsten content seems to increase between 6.5 and 15 μm below the surface. The inner rim contains the same elements as the outer rim, although enriched in tungsten. No inner rim was found in the region down to 7 μm below the surface. From there and downwards no direct relation between depth and composition of the inner rim is evident.

The nitrogen-rich phase is present only in the surface zone of the heat-treated material and surrounds the carbonitride grains. The grain shape of this phase is often irregular and most of the rim seems to have been consumed in the regions where the nitrogen-rich phase appears. Apart from titanium, nitrogen and carbon, this phase also contains small amounts of tungsten. The nitrogen content of the nitrogen-rich phase decreases with increasing depth, whereas titanium and tungsten increase. The carbon content does not vary with depth. Consequently, the C+N content decreases with increasing depth. The nitrogen-rich

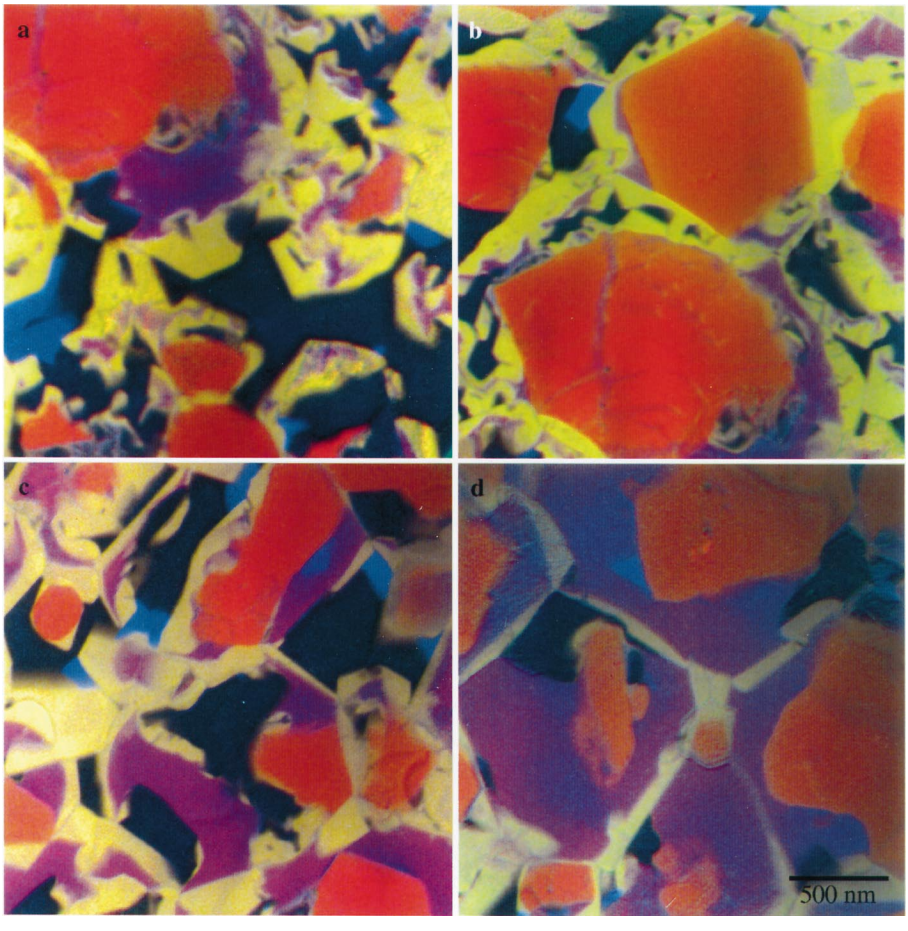

Fig. 4. RGB images from different depths of the heat-treated cermet. (a) 0–3 μm; (b) 2–5 μm; (c) 5–8 μm; and (d) 8–11 μm below the surface. Titanium—red; nitrogen—green; tungsten—blue.

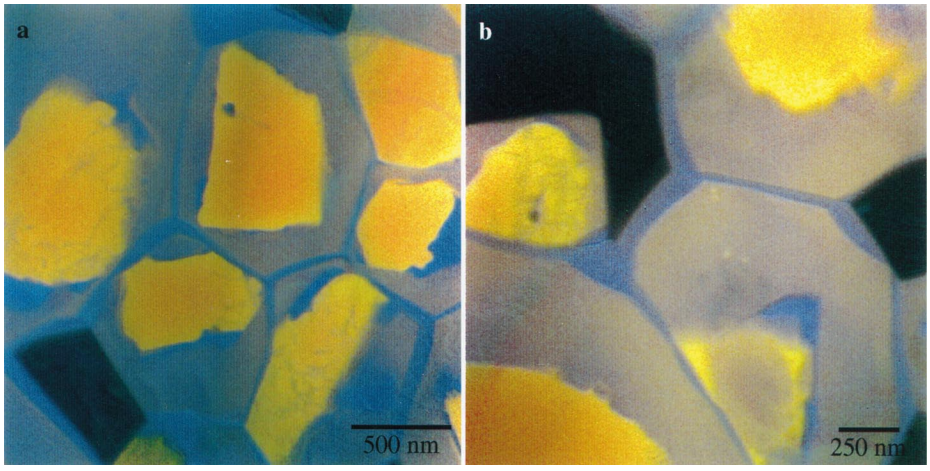

Fig. 5. RGB images from (a) 100 μm and (b) 150 μm below the surface of the heat-treated material. Titanium—red; nitrogen—green; tungsten—blue.

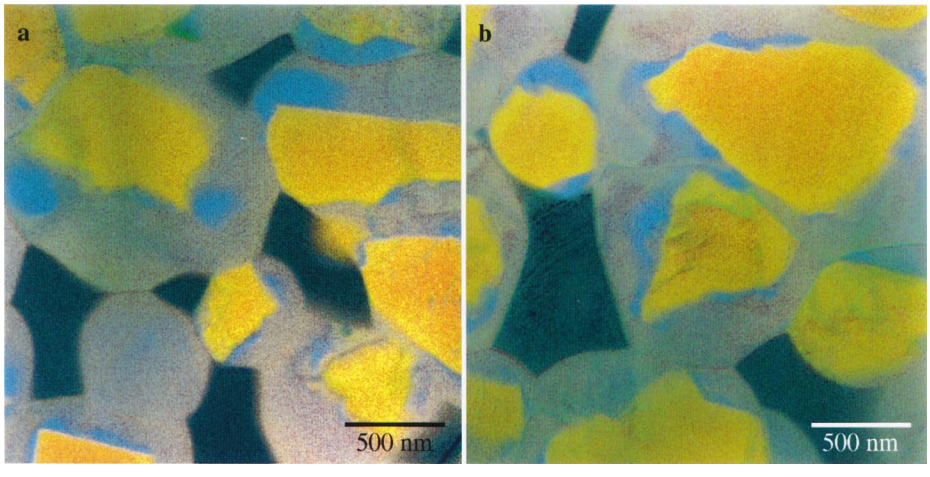

Fig. 6. RGB images from (a) the surface zone and (b) the bulk of the as-sintered material. Titanium—red; nitrogen—green; tungsten—blue.

Table 2. Binder phase composition at different depths from the surface of the heat-treated material as determined by TEM/EDX/EELS (given in at%). Each value is a mean value of 5–15 point analyses

Binder	Ti (at%)	W (at%)	C (at%)	N (at%)	Co (at%)
1.5 μm	1.7±0.2	6.8±0.3	–	–	91.5±0.7
3.8 μm	1.5±0.4	5.8±0.5	–	–	92.7±0.9
6.0 μm	1.4±0.2	5.0±0.6	–	–	93.6±0.5
8.6 μm	1.5±0.5	5.5±0.3	–	–	93.0±0.8
9.8 μm	1.8±0.3	5.6±0.4	–	–	92.6±0.6
15 μm	1.9±0.5	5.6±0.5	–	–	92.5±0.6
20 μm	1.0±0.6	6.5±0.4	–	–	92.5±0.7
150 μm	0.7±0.3	4.2±0.4	–	–	95.1±0.5

phase is found down to approximately 15 μm below the surface.

Some tungsten-rich phases that are not usually present in cermet materials were observed in the heat-treated material. Close to the surface, small grains of tungsten carbide have been formed during the heat-treatment, and η-phase was found to be present at a depth of about 15 μm. The tungsten-rich (Ti,W)(C,N) phase at 100 μm depth has grown onto the carbonitride grains and has a morphology similar to the

Table 3. Composition of the core at different depths from the surface of the heat-treated material as determined by TEM/EDX/EELS (given in at%). Each value is a mean value of 5–15 point analyses

Core	Ti (at%)	W (at%)	C (at%)	N (at%)	Co (at%)
1.4 μm	50.8±0.3	–	30.9±0.3	18.3±0.4	–
3.4 μm	51.4±0.5	–	31.5±0.3	17.1±0.2	–
5.9 μm	51.1±0.3	–	31.3±0.2	17.6±0.4	–
7.2 μm	51.3±0.6	–	31.5±0.5	17.2±0.3	–
8.5 μm	51.5±0.4	–	31.5±0.4	17.0±0.5	–
15 μm	52.5±0.7	–	30.4±0.9	17.1±0.6	–
20 μm	53.9±0.5	–	28.7±0.6	17.4±0.4	–
150 μm	54.0±0.5	–	29.0±0.5	17.0±0.7	–

Table 4. Composition of the outer rim at different depths from the surface of the heat-treated material as determined by TEM/EDX/EELS (given in at%). Each value is a mean value of 5–15 point analyses

Outer rim	Ti (at%)	W (at%)	C (at%)	N (at%)	Co (at%)
1.2 μm	45.7±0.6	6.0±1.0	32.6±1.5	15.7±0.5	–
3.5 μm	46.3±0.6	5.5±0.7	33.4±0.4	14.8±0.8	–
6.5 μm	46.2±0.3	7.0±0.5	33.5±0.3	13.3±0.9	–
8.5 μm	47.0±0.3	6.0±0.3	33.9±0.6	13.1±0.6	–
15 μm	47.5±0.8	5.6±0.4	33.6±0.5	13.3±0.7	–
20 μm	46.0±0.4	6.2±0.6	32.9±0.8	14.9±0.6	–
150 μm	45.2±0.5	6.9±0.7	33.0±0.6	14.9±0.2	–

Table 5. Composition of the inner rim at different depths from the surface of the heat-treated material as determined by TEM/EDX/EELS (given in at%). Each value is a mean value of 5–15 point analyses

Inner rim	Ti (at%)	W (at%)	C (at%)	N (at%)	Co (at%)
7.1 μm	39.2±0.5	15.2±0.4	39.8±0.9	5.8±0.4	–
9.2 μm	37.4±0.3	19.2±0.5	37.0±0.6	6.4±0.7	–
15 μm	39.2±0.8	15.9±0.6	38.8±0.7	6.1±0.9	–
20 μm	38.0±0.6	18.8±0.9	37.0±0.5	6.2±0.5	–
150 μm	38.9±0.5	16.2±0.5	40.0±0.7	4.9±0.7	–

Table 6. Composition of the nitrogen-rich phase at different depths from the surface of the heat-treated material as determined by TEM/EDX/EELS (given in at%). Each value is a mean value of 5–15 point analyses

N-rich phase	Ti (at%)	W (at%)	C (at%)	N (at%)	Co (at%)
1.6 μm	47.9±0.5	0.5±0.8	13.5±0.4	38.1±0.6	–
3.7 μm	47.8±0.4	0.9±0.3	13.7±0.7	37.6±0.5	–
5.8 μm	47.8±0.3	1.5±0.6	13.7±0.3	37.0±0.8	–
8.1 μm	49.5±0.5	1.9±0.3	14.2±0.8	34.4±0.4	–
15 μm	51.7±0.4	2.8±0.5	14.6±0.6	30.9±0.5	–

Table 7. Composition of the tungsten-rich phases (WC, η-phase and (Ti,W)(C,N)) at different depths from the surface of the heat-treated material as determined by TEM/EDX/EELS (given in at%). Each value is a mean value of 5–15 point analyses. NA = not analysed

W-rich phases	Ti (at%)	W (at%)	C (at%)	N (at%)	Co (at%)
4.3 μm	–	100 metal	NA	NA	–
15 μm	9.6 metal	46.9 metal	NA	NA	43.5 metal
150 μm	40.8±0.8	12.0±0.5	38.7±0.6	8.5±0.8	–

nitrogen-rich phase present in the surface zone, although it is more regularly distributed on the carbonitride grains.

3.2. Thermodynamic calculations

The core–rim microstructure of the as-sintered cermet indicates that the system is far from equilibrium. However, the binder phase is locally in contact with all the different constituents and it seems reasonable to assume that binder and phases dissolved and reprecipitated during the heat-treatment are close to thermodynamic equilibrium.

The calculated equilibrium nitrogen activity at 1200°C for the composition according to Table 1 is 0.0195 $bar^{1/2}$, corresponding to a partial pressure of N_2 of 0.38 mbar. The equilibrium state corresponds to a carbon activity of 0.91 relative to graphite. The transport of carbon in the binder is much faster compared to other elements in the alloy. The transport of nitrogen is limited due to a very low solubility and the transport of metallic elements due to low diffusivities. The carbon activity will, thus, be close to constant in the specimen during the nitriding heat-treatment. A property diagram showing the constitution as a function of nitrogen activity can be found in Fig. 7. The calculation was performed under the constraints of constant carbon activity of 0.91 and constant amounts of metallic elements. Note that tungsten carbide will precipitate if the nitrogen activity is above 0.14 $bar^{1/2}$. The composition of the reprecipitated carbonitride phase as a function of nitrogen activity calculated under the same constraints is shown in Fig. 8.

A difference in nitrogen activity between the surface, 1 $bar^{1/2}$, and the centre, 0.0195 $bar^{1/2}$ at constant carbon activity will result in a difference in activity for the metallic elements. Calculated ratio of activity between the centre and the surface for all the elements is presented in Table 8. There is a strong driving force for transport of titanium towards the surface and nitrogen towards the centre and a somewhat lower driving force for tungsten transport towards the centre.

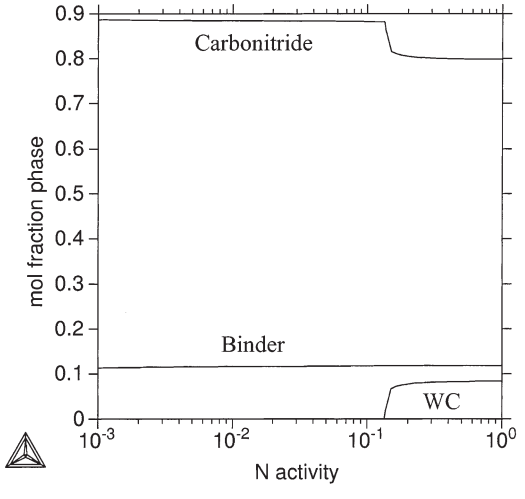

Fig. 7. Calculated constitution as a function of nitrogen activity at 1200°C. The carbon activity is 0.91 and the amounts of metallic elements are kept constant.

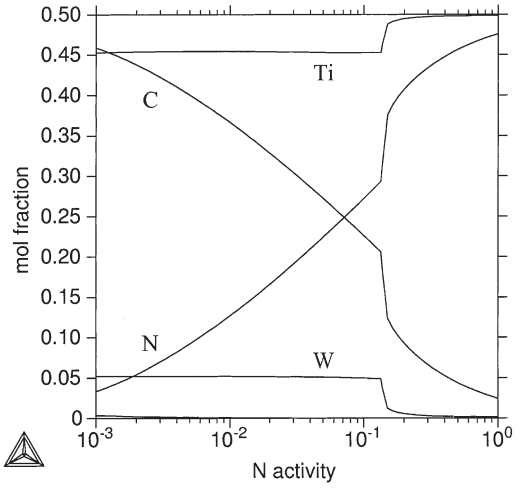

Fig. 8. Calculated composition of the carbonitride phase as a function of nitrogen activity at 1200°C. The carbon activity is 0.91 and the amounts of metallic elements are kept constant.

Table 8. Calculated ratio of chemical activity for the elements in the bulk and at the surface

C	Co	N	W	Ti
1.00	1.02	0.0195	0.226	18.0

3.3. Performance

The result of the cutting tests is shown in Fig. 9. The data points represent the average of two cutting edges for each variant. The most interesting feature in the diagram is the slope of the curves. A lower slope represents better plastic deformation resistance. Clearly, the nitrided insert performs quite well in this

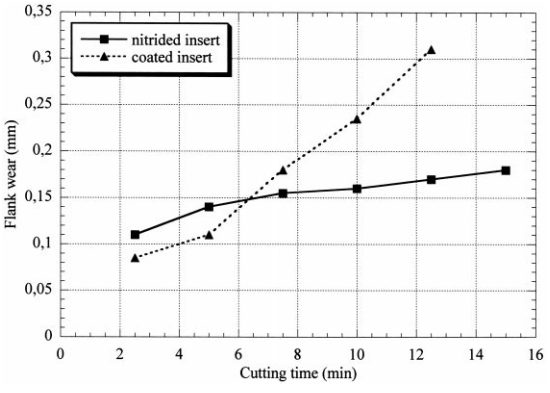

Fig. 9. Plastic deformation resistance in longitudinal turning of steel. The deformation causes edge impression and is detected by measuring the flank wear *VB* (mm) as a function of cutting time (min).

respect. It should be noted that in the as-sintered state, the same material will undergo fracture induced by plastic deformation in less than 2.5 min. Thus the improvement is dramatic.

In the toughness test the PVD-coated reference obtained an average tool life of 33 passes while the nitrided inserts obtained an average tool life of 34 passes. Three cutting edges were tested for each variant. In this type of gentle toughness test, dominated by thermal cycling, the nitrided material performs on a par with a tough PVD-coated grade.

4. DISCUSSION

4.1. Microstructure

The microstructural characterisation has been concentrated on the surface zone of the heat-treated cermet material. The as-sintered material has been studied mainly for comparison.

4.1.1. Binder phase. Since diffusion is substantially faster in the cobalt binder than in carbonitrides, the binder will act as the main transport medium during the heat-treatment. The increased nitrogen activity will cause dissolution of carbonitride phases in the binder and reprecipitation of new phases (Fig. 7). The electron microprobe depth profiles show that there is an increase in cobalt at the surface and a bump in the cobalt curve between 15 and 40 μm below the surface. It should be noted that, due to the limited spatial resolution of the method and the fine-grained materials to be analysed, the depth profiles provided by EMPA show the average composition of all phases (weighted by their volume fractions) present at the different depths in the material. This means that since the binder phase is the only cobalt-containing phase and its cobalt content increases with depth, the bump in the cobalt curve must be due to a change in volume fraction of the binder phase. The cobalt bump appears just below the region enriched in titanium-based phases and is to be interpreted as an inward diffusion of cobalt caused by the outward transport of titanium-rich phases. The increase in cobalt close to the surface is evidently not an effect of the heat-treatment itself since this increase is also found in the as-sintered material.

4.1.2. WC and η-phase. Both tungsten carbide and η-phase present in the surface zone of the heat-treated material seem to have nucleated from the binder phase and have a shape similar to that of the binder. These tungsten-rich phases reprecipitate from the supersaturated solid solution. They have not been allowed to grow freely, and grain growth is apparently limited by the surrounding carbonitride grains. The formation of tungsten carbide in the surface zone with high nitrogen activity is predicted by the thermodynamic calculations (Fig. 7). According to the thermodynamic models, η-phase can only form at carbon activity of less than approximately 0.25 at 1200°C. The assumption of a constant carbon activity of 0.91 results in no formation of η-phase. At present, the formation of η-phase cannot be explained from thermodynamic calculations.

4.1.3. Carbonitride phases. The high nitrogen activity in the surface region forces tungsten-rich phases, i.e. inner and outer rim, to dissolve into the binder. In as-sintered cermets, the inner rim is usually trapped between the core and the outer rim, whereas the outer rim frequently borders on the binder phase. Hence, preferentially the outer rim is dissolved during the early stages of the heat-treatment. Later on, as the thickness of the outer rim decreases, the inner rim is released for dissolution as well. It is reasonable to believe that the dissolution of the inner rim, once started, goes faster than the dissolution of the outer rim, considering that the driving force exerted by the nitrogen activity is higher for the inner rim as a consequence of its higher tungsten content. This is supported by the fact that almost no inner rim was found to be present down to 15 μm depth, and was never in contact with the binder phase. During dissolution of the rim not only tungsten but also titanium is set free. Tungsten is driven inwards, while titanium stays or diffuses outwards to form titanium-rich phases. Both fluxes are caused by the high nitrogen activity at the surface, as demonstrated by the thermodynamic calculations of activity ratios for titanium and tungsten in Table 8.

4.1.4. N-rich carbonitride. The most obvious result of the heat-treatment is the formation of the nitrogen-rich phase that appears very frequently in the surface zone, down to approximately 15 μm depth. The composition of this phase differs from the carbonitride phases usually present in cermet materials by being mainly composed of titanium and nitrogen. Smaller amounts of carbon and tungsten are also present. This is in accordance with the thermodynamic calculations in Fig. 8, and the phase composition corresponds to the equilibrium composition at a nitrogen activity where tungsten carbide has just formed. The nitrogen-rich phase has reprecipitated and grown on already existing carbonitride grains, first on the outer rim and later on, when most of the outer rim is dissolved in the binder, also on the cores. The shape of the nitrogen-rich phase is irregular, and it is often present as a surrounding layer on core–rim structured carbonitride grains. The atoms that form this phase originate from the nitrogen atmosphere and from the previous carbonitride grains that have been dissolved in the binder. The low solubility of nitrogen in the cobalt binder is the reason why this phase is concentrated to a quite thin surface region. Titanium is transported from the inner parts of the material to supply the formation of the nitrogen-rich phase in the surface zone.

4.1.5. W-rich carbonitride. A few hundred microns below the surface of the heat-treated material the microstructure appears more like cermet micro-

structures usually do, with the addition of the tungsten-rich phase surrounding the core–rim structured carbonitride grains as the only difference. This phase cannot be a result of inward diffusion of tungsten only (as a consequence of the high nitrogen activity in the surface zone), since it is found at distances from the surface that exceeds the diffusion length of tungsten in cobalt at 1200°C by a factor of five (calculated from the diffusion coefficient for dilute solutions of tungsten in fcc cobalt suggested by Ruzickova *et al.* [20]). The solubility of nitrogen in the binder is very low and thereby the inward diffusion of nitrogen in the binder is limited. Instead, the high nitrogen activity close to the surface causes outward diffusion of titanium to enable the formation of the nitrogen-rich carbonitride phase. It is therefore likely that the heat-treatment causes dissolution of titanium-containing phases at depths well below the surface to make titanium available for diffusion to the surface region. The diffusion length of metal atoms is much larger in the binder phase than in the carbonitride phases, which means that diffusion mainly takes place through the binder. Most of the titanium-containing phases that are in contact with the binder phase in a cermet material also contain tungsten. When titanium is transported towards the surface tungsten remains, and consequently, reprecipitation onto the carbonitride grains results in a more tungsten-rich surrounding phase. It should be noted that this phase is not present on all carbonitride grains on the surfaces that are in contact with the binder phase, which substantiate that some carbonitride grains are under dissolution during the heat-treatment while others grow due to reprecipitation.

4.2. Performance

In this work, performance has been evaluated using two different turning operations testing plastic deformation resistance and toughness. This is not sufficient to draw any conclusions concerning the performance level in general of this type of material compared to conventional cermets, but this has not been our ambition. However, the tests do demonstrate that the heat-treatment leads to a dramatic improvement in plastic deformation resistance and that this is achieved without obtaining a catastrophic embrittlement of the material. The question then arises if this improvement can be explained with the aid of the microstructural characterisation reported above.

The most striking result of the heat-treatment is certainly the growth of a titanium- and nitrogen-rich phase onto existing carbonitride grains in the surface zone. This phase not only differs in composition compared to the carbonitride phases usually present in cermet materials, but also changes the morphology of the carbonitride grains from a relatively rounded shape to quite irregular, often interlocking shapes. Bolognini *et al.* [21] have described the deformation of cermets in terms of three different regions with respect to temperature. At low temperature the material is brittle. As the temperature is raised, limited deformation starts to occur due to plastic deformation of the hard phase. Finally, at sufficiently high temperature, more extensive deformation is obtained due to grain boundary sliding. Certainly, this last region is most important for plastic deformation in cutting tool applications. Assuming that grain boundary sliding dominates, it seems reasonable that the onset of this deformation mode can be shifted to higher temperatures by the morphological changes to interlocking grain shapes obtained in the surface zone of the heat-treated cermet.

5. CONCLUSIONS

- The heat-treatment in nitrogen introduced a 20 μm surface zone enriched in nitrogen and titanium and deficient in tungsten and carbon. However, the microstructure is influenced by the heat-treatment down to at least 150 μm below the surface.
- The heat-treatment caused dissolution of tungsten containing carbonitride phases in the binder. Dissolved atoms are transported through the binder, titanium towards the surface and tungsten inwards, and reprecipitate onto carbonitride grains, the driving force being the nitrogen activity. The composition of the reprecipitated phases depends on the local equilibrium at the different depths.
- In the region close to the surface, down to 15 μm, the heat-treatment caused the formation of a nitrogen-rich phase. This phase is a carbonitride, rich also in titanium and with smaller amounts of carbon and tungsten. It has reprecipitated onto already existing carbonitride grains and often forms a surrounding layer with an irregular shape. The titanium present in this phase has been transported from the inner part of the material towards the region of high nitrogen activity.
- Small grains (about 150 nm) of tungsten carbide and η-phase have formed in the surface zone during the heat-treatment. These phases are always in contact with the binder phase and have a grain morphology similar to that of the binder.
- A tungsten-rich carbonitride phase was observed to form a thin layer on the carbonitride grains down to at least 150 μm below the surface of the heat-treated material. The composition of this phase cannot be explained by inward diffusion of tungsten, but is rather an effect of the outward transport of titanium.
- Thermodynamic calculations show that tungsten carbide as well as a nitrogen- and titanium-rich carbonitride phase is formed in the surface zone of the heat-treated cermet. Diffusion of titanium towards the surface and of nitrogen and tungsten towards the centre is predicted. The driving force for titanium diffusion towards the surface is significantly larger than the driving force for tungsten diffusion towards the interior.

- The heat-treatment leads to a dramatic improvement in plastic deformation resistance. This is explained by the change in morphology of the hard phase grains in the surface region from rounded grains to irregular, often interlocking shapes.

Acknowledgements—Financial support from the Swedish Research Council for Engineering Science (TFR) is gratefully acknowledged.

REFERENCES

1. Suzuki, H., Taniguchi, Y., Hayashi, K. and Sanuan, C. *J. Jpn. Inst. Met.*, 1981, **45**, 95–99.
2. Schwarzkopf, M., Exner, H. E., Fischmeister, H. F. and Schintlmeister, W. *Mater. Sci. Engng*, 1988, **A105–106**, 225–231.
3. Gustafson, P. and Östlund, Å. *Int. J. Refr. Met. Hard Mater.*, 1993, **12**, 129–136.
4. Yohe, W. C. *Int. J. Refr. Met. Hard Mater.*, 1993, **12**, 137–144.
5. Zackrisson, J., Rolander, U., Weinl, G. and Andrén, H. -O. *Int. J. Refr. Met. Hard Mater.*, 1998, **16**, 315–322.
6. Konyashin, I. Y. *Surf. Coat. Technol.*, 1995, **73**, 125–131.
7. Snell, P. O. *Planseeberichte für Pulvermetallurgie*, 1974, **22**, 91–106.
8. Heuer, A. H., Sears, J. S. and Zaluzec, N. J. in *Proceedings of the International Conference on the Science of Hard Materials* 2, ed. E. A. Almond, C. A. Brookes and R. Warren. Adam Hilger Ltd, Bristol and Boston, 1986, pp. 321–334.
9. Sundman, B., Jansson, B. and Andersson, J. O. *Calphad*, 1984, **9**, 153–190.
10. Reimer, L. *Energy-filtering Transmission Electron Microscopy*, Springer-Verlag, Berlin, Heidelberg 1995.
11. Zackrisson, J., Grogger, W., Hofer, F. and Andrén, H. -O. *Ultramicroscopy*, 1999, **79**, 273–281.
12. Ekroth, M., Frisk, K., Jansson, B. and Dumitrescu, L. F. S. *Metall. Mater. Trans. B*, 2000, **31B**, 615–619.
13. Stjernberg, K. G. *Powder Metallurgy*, 1970, **13**, 1–12.
14. Doi, H. in *Proceedings of the International Conference on the Science of Hard Materials*, ed. Z. Rhodes, E. A. Almond, C. A. Brookes and R. Warren, Adam Hilger Ltd, Bristol and Boston 1986, pp. 489–523.
15. Lindau, L. and Stjernberg, K. G. *Powder Metallurgy*, 1976, **19**, 210–213.
16. Yoshimura, H., Sugizawa, T., Nishigaki, K. and Doi, H. *Int. J. Refr. Met. Hard Mater.*, 1983, **33**, 170–174.
17. Lindahl, P., Gustafson, P., Rolander, U., Stals, L. and Andrén, H.-O., *Int. J. Refr. Met. Hard Mater.*, 1999, **17**, 411–421
18. Zackrisson, J., Rolander, U. and Andrén, H.-O., *Metall. Mater. Trans. A*, in press.
19. Zackrisson, J. and Grogger, W., *J. Electron Microscopy*, submitted for publication.
20. Ruzickova, J., Million, B. and Kucera, J. *Kovove Materialy*, 1981, **19**, 3.
21. Bolognini, S., Feusier, G., Mari, D., Viatte, T. and Benoit, W. *Int. J. Refr. Met. Hard Mater.*, 1998, **16**, 257–268.